Personalized Intrinsic Network Topography Mapping and Functional Connectivity Deficits in Autism Spectrum Disorder

Supplemental Information

Technical Methods

- Preprocessing Pipeline
- Supplemental Table S1. Loadings from a principal component analysis of the temporal scan quality metrics derived from the quality assurance pipeline (QAP).
- The PINT Algorithm
- Supplemental Table S2. Locations of the PINT ROIs.

ABIDE I Methods and Results

- Method
  - Sample Preprocessing Pipeline and Quality Assurance
- Supplemental Table S3. Scanning parameters and participant demographics across sites.
- Results
  - Performance of the PINT Algorithm in ABIDE I
  - Whole Brain Network Correlation Maps
- Supplemental Figure S1. Whole brain correlations with template vertex seeds.
- Supplemental Figure S2. Whole brain correlations with personalized vertex seeds.
- Supplemental Figure S3. Probabilistic maps of personalized ROI locations by network.
- Supplemental Figure S4: No effect of in scanner head motion on PINT vertex displacement.
- Supplemental Figure S5. Average correlation matrices (Z-transformed) from ABIDE I participants (n=889) calculated A) before PINT correlation ("template" ROIs) and B) after PINT correction ("personalized" ROIs).
- Supplemental Table S4. Mean (SD) network correlation (Z-transformed) from n=889 ABIDE I participants for template (Before PINT) and personalized (After PINT) ROIs.
- Supplemental Figure S6. Within ROI heterogeneity in resting state network correlation decreases with the application of PINT.
- Supplemental Table S5. Association of ADOS total score with functional connectivity (n=264).
- Supplemental Figure S8. Edges showing where a significant (FDR corrected) negative correlation between intrinsic connectivity and ADOS total scores was observed.

CoRR and ABIDE Longitudinal

- Methods

Datasets
Supplemental Table S6. Demographic information from the CoRR participants employed in this analysis.
Preprocessing Workflow
Test-Retest Analysis of Resting State Connectivity
Supplemental Figure S9. Between-subject and within-subject distance for personalized ROI locations by network.
Supplemental Table S7. Paired t-test results for within-subject and between-subject distances of PINT personalized ROI locations across site and diagnosis.
Supplemental Table S8. Comparison of within subject and cross subject correlation matrices, before and after PINT.
Evaluation of PINT Parameters on Test-Retest Performance
Methods
Results
Supplemental Figure S10: Evaluating the effects of PINT input parameters on test-retest reliability of PINT results (n=158 test-retest participants).
Table S9. Effects of ASD Diagnosis on vertex displacement and functional correlations after varying the PINT sampling radius settings.
Supplemental Figure S11. Maximizing full correlation within the PINT algorithm increases the correlation (adjusted for scanning site and age) between functional connectivity and head-motion (mean framewise displacement), but maximizing partial correlation does not increase correlation between functional connectivity and head-motion.
Supplemental References

Technical Methods

Preprocessing Pipeline

The T1w images were submitted to FreeSurfer's recon-all pipeline (1)(v.5.3.0, http://surfer.nmr.mgh.harvard.edu/). The FreeSurfer outputs (surfaces and cortical thickness values) were then converted to GIfTI and CIfTI format using scripts adapted from the Human Connectome Project's (HCP) Minimal Processing Pipeline (2). These adapted scripts are available at https://github.com/edickie/ciftify (see bin/ciftify_recon_all). Following conversion, as in the HCP Minimal Processing Pipeline, all surfaces were transformed to the MNI template using FSL FNIRT (3), and the left and right surfaces within each individual were then registered to each other using FreeSurfer and re-sampled to a 32k mesh. Therefore all subjects were analyzed in HCP's "MNINonLinear-fsaverage_LR32 space". Resting state functional images were preprocessed using a combination of tools from AFNI (4) (https://afni.nimh.nih.gov/afni/, last update 2015.12.15) and FSL (3) (v.5.0.9; http://fsl.fmrib.ox.ac.uk/fsl/fslwiki/FSL), which were combined using an in-house pipeline tool (https://github.com/josephdviviano/epitome). Preprocessing steps were as follows: 1) the first three volumes were removed; 2) temporal spikes (defined as timepoint outliers larger than 2.5 standard deviations from a 5 term polynomial fit to each voxel's time series) were removed using AFNI's 3dDespike; 3) slice timing correction was completed using AFNI's 3DTshift; 4) the global mean of the image was set to 1000; 5) motion correction was completed using AFNI's 3dvolreg; 6) signal from outside the brain was removed from the EPI image using FSL's BET; 7) the linear trend was removed from each timeseries; 8) removal of artefacts was conducted using ICA-FIX (5). For the ICA data cleaning step, 18 FIX classifiers (one for each sample included in the analysis) were trained using labels from a random set of 25 participants from each site. To facilitate this process, ICA components from the training set were first labeled using the 'Standard' training set available with ICA FIX. These labels were then readjusted with the aid of an in-house html quality control interface (https://github.com/edickie/icarus). Following data cleaning, fMRI images were non-linearly transformed to MNIspace, and then resampled to MNINonLinear-fsaverage_LR32 space. Finally, the fMRI data was smoothed along the cortical surface, and subcortical ROIs were smoothed within-parcel, both using a

8mm full-width half-max (FWHM) Gaussian kernel.

Quality assurance metrics for the resting state scans were assessed using the Quality Assurance Pipeline (https://github.com/preprocessed-connectomes-project/quality-assessment-protocol 20160715). Participants were excluded for having a framewise displacement greater than 1mm for greater than 5 percent of the resting state scan and/or having less than 6 "signal" ICA components (labeled by ICA-FIX) in the resting state scan (see ABIDE I Methods and Results section, below, for numbers excluded). After excluding scans of low quality, quality assurance metrics from the remaining participants were transformed to normality and submitted to a principal component analysis. The top two principal components accounted for a total of 83% of the variance in temporal scan quality (variable loadings are given in Supplemental Table S1). The second component (PC2) is dominated by motion (mean framewise displacement). The first component showed stronger loadings from the other three metrics of scan quality. These two scan quality QC's principle components were included as covariates in all subsequent analyses.

Supplemental Table S1. Loadings from a principal component analysis of the temporal scan quality metrics derived from the quality assurance pipeline (QAP).

These two PC's were included as covariates in all subsequent analyses.

	PC 1 (54.4 % of Variance)	PC2 (28.9 % of Variance)
DVARS[a]	-0.492	-0.478
Mean Temporal Signal to Noise Ratio	**-0.618**	-0.156
Mean Framewise Displacement	0.214	**-0.821**
Median Distance Index[b]	**-0.574**	0.272

[a] The average change in mean intensity between each pair of fMRI volumes in a series scaled to make comparisons across scanning protocols possible. Lower values are better (6) http://blogs.warwick.ac.uk/nichols/entry/standardizing_dvars.
[b] Calculated using AFNI's 3dTqual (4).

The PINT Algorithm

PINT fits an individual participant's resting connectivity matrix to a "template" pattern of networks by moving the locations for sampling ROIs in a manner that optimizes the within-network connectivity. The code is available at https://github.com/edickie/ciftify, see ciftify-PINT-vertices). We build upon the result, from brain stimulation site targeting, that correlation with a network average timeseries, constructed as an average from multiple dispersed regions of the same network, can more reliably locate a functional region of interest than correlation with one ROI alone (7). Therefore, we define our network average timeseries as that calculated from all ROIs of the same network, excluding the ROI being localized. We maximise partial correlation between the target ROI and the network average timeseries (controlling for the average network timeseries from the other five networks). We maximise partial correlation, rather than full correlation, because of reports that partial correlation measures are less susceptible to motion artefacts (8, 9).

PINT works in an iterative fashion. It starts by calculating average mean timeseries from circular ROIs (of 6mm radius) around 80 central "template" vertices. Then, for each template vertex, search area is defined as those vertices within 6mm of the central template vertex and not within 12mm of any other ROI's template vertex. PINT then calculates the partial correlation of all vertices within search area around the template vertex and average timeseries from the other ROIs of the same network (the partial correlation controls for the five average timeseries of the ROIs of the other networks). The center of the ROI is moved to the vertex within the 6mm radius search space with the maximal partial correlation to the remaining within-network ROIs. Once all 80 ROIs have been moved to the vertices of highest partial correlation, the algorithm iterates, updating the network timeseries and searching around the new vertex locations. The algorithm stops when all 80s ROIs are centered around the vertex is that of maximal partial correlation with those of the same network, or after 50 iterations (whichever comes first).

Performance of the PINT algorithm in the ABIDE I sample showed that resolves within an average of 14 iterations (max: 36 iterations, see " ABIDE I Dataset - Results.")

Using the CoRR test-retest data, we experimented with which PINT radius parameters would yield the highest test-retest results. Results are reported in Evaluating PINT Parameters.

Supplemental Table S2. Locations of the PINT ROIs.

Network	Lobe	hemi	MNI coordinate x	y	z	Template Vertex ID	Abbreviation
Dorsal Attention Network (DA)	Frontal	L	-27	-4	52	6111	DAF1L
		R	27	-6	51	6141	DAF1R
		L	-49	4	31	19598	DAF2L
		R	49	6	28	19537	DAF2R
	Parietal	L	-29	-72	31	13828	DAP1L
		R	34	-68	34	13828	DAP1R
		L	-24	-58	60	14785	DAP2L
		R	18	-60	62	12052	DAP2R
		L	-44	-34	42	7417	DAP3L
		R	49	-30	44	7507	DAP3R
	Temporal	L	-47	-64	-2	23315	DAT1L
		R	53	-58	-5	23315	DAT1R
Default Mode Network (DM)	Frontal	L	-32	21	48	30442	DMF1L
		R	16	40	46	27830	DMF1R
		L	-6	58	21	28834	DMF2L
		R	6	58	21	28834	DMF2R
		L	-9	46	-4	28175	DMF3L
		R	9	44	-5	28175	DMF3R
	Parietal	L	-11	-50	32	13363	DMP1L
		R	7	-56	29	11809	DMP1R
		L	-47	-60	30	16429	DMP2L
		R	50	-59	26	16195	DMP2R
	Temporal	L	-58	-37	-3	9000	DMT1L
		R	58	-31	-3	9000	DMT1R
		L	-61	-10	-19	32170	DMT2L
		R	61	-6	-17	32221	DMT2R
Fronto-Parietal Network (FP)	Frontal	L	-6	24	41	2465	FPF1L
		R	6	25	43	2424	FPF1R
		L	-22	11	53	30321	FPF2L
		R	24	11	53	30321	FPF2R
		L	-43	23	33	30458	FPF3L
		R	45	24	34	30458	FPF3R
		L	-37	46	15	29627	FPF4L
		R	36	54	6	19783	FPF4R
		L	-33	19	-6	10957	FPF5L
		R	31	24	-6	11073	FPF5R
	Parietal	L	-7	-71	44	12812	FPP1L

		R	8	-70	46	12848	FPP1R
		L	-48	-48	48	6841	FPP2L
		R	40	-55	45	13895	FPP2R
	Temporal	L	-56	-50	-17	22055	FPT1L
		R	59	-40	-15	21912	FPT1R
Ventral Attention Network (VA)	Frontal	L	-9	9	37	2453	VAF1L
		R	9	10	39	2411	VAF1R
		L	-10	-1	69	3469	VAF2L
		R	11	-1	70	3469	VAF2R
		L	-46	-3	50	5450	VAF3L
		R	52	1	45	30946	VAF3R
		L	-53	8	1	18804	VAF4L
		R	55	9	3	18804	VAF4R
		L	-30	40	29	29837	VAF5L
		R	29	44	26	29591	VAF5R
	Insula	L	-37	9	-1	10782	VAI1L
		R	40	12	-2	10782	VAI1R
	Parietal	L	-15	-33	40	4089	VAP1L
		R	14	-30	40	4130	VAP1R
		L	-61	-30	26	17169	VAP2L
		R	61	-35	32	9371	VAP2R
	Temporal	L	-53	-58	8	15764	VAT1L
		R	56	-50	8	15844	VAT1R
Sensory Motor Network (SM)	Frontal	L	-4	-16	56	4632	SMF1L
		R	5	-15	56	4632	SMF1R
		L	-26	-31	60	7662	SMF2L
		R	26	-29	60	7662	SMF2R
		L	-54	-12	33	17981	SMF3L
		R	54	-9	33	17981	SMF3R
	Insula	L	-38	-14	11	10427	SMI1L
		R	40	-11	11	10427	SMI1R
		L	-59	-15	5	31742	SMT1L
		R	60	-9	3	31742	SMT1R
Visual Network (VI)	Occipital	L	-36	-84	6	15123	VI01L
		R	41	-79	6	15123	VI01R
		L	-16	-90	23	11965	VI02L
		R	22	-87	24	11965	VI02R
		L	-2	-85	10	25314	VI03L
		R	5	-83	12	25314	VI03R
		L	-11	-81	-10	24579	VI04L
		R	13	-77	-8	24579	VI04R
		L	-27	-62	-11	24616	VI05L
		R	28	-57	-12	24616	VI05R

ABIDE I Methods and Results

Method

Sample Preprocessing Pipeline and Quality Assurance

ASD and TD resting state intrinsic connectivity was tested using the ABIDE dataset (ABIDE I release) (10). ABIDE is a publicly available multi-site dataset combining 17 scanning sites. Each site acquired a resting state fMRI and a T1-weighted anatomical scan. For details of the scanning parameters for each individual site see, http://fcon_1000.projects.nitrc.org/indi/abide/abide_I.html. Phenotypic information of diagnosis, sex, full-scale IQ and ADOS scores were taken from the ABIDE I phenotypic file for analyses. Data from the OHSU site were not included because the shorter duration of the resting state scans was not suitable for FSL's ICA-FIX denoising (see Preprocessing Methods section, above). Data from the Stanford site were excluded due to poor quality of the anatomical images leading to a poor performance of the FreeSurfer pipeline. Demographic criteria from participants included in our analyses (n=393 ASD, n=496 TD, across 15 sites, ages 6-65) are described in Supplemental Table S2. Full-scale IQ was imputed, if not available, using the mean value from each participant's site and diagnostic group (ASD vs TD).

Preprocessing of images was completed as described in the 'Preprocessing Pipeline' section, above. Quality assurance metrics for the resting state scans were assessed using the Quality Assurance Pipeline (pulled from https://github.com/preprocessed-connectomes-project/quality-assessment-protocol 20160715). Following QC, 393 of 539 ASD participants and 496 of 573 TD participants were included in our analysis (for demographic criteria; see Supplemental Table S2). Participants were excluded for the following reasons: having a poor quality anatomical scan that failed FreeSurfer surface segmentation (n=128), failing to have full cortex coverage during the resting state scan (n=22), having a resting state scan with a framewise displacement greater than 1mm for greater than 5 percent of the resting state scan and/or having less than 6 "signal" ICA components (labeled by ICA-FIX) in the resting state scan (n=63).

Supplemental Table S3. Scanning parameters and participant demographics across sites.

				n		Age	FIQ		ADOS
Site	Scanner	#TR	TR(ms)	TD:ASD	%Male	Range	ASD M(SD)	TD M(SD)	M(SD)
SDSU	GE	180	2000	21:6	77.80	8.7-17.1	124.5(13.0)	108.0(10.8)	12.5(4.6)
UM	GE Signa (Spiral)	300	2000	67:45	78.60	8.2-28.8	108.4(17.7)	108.3(9.7)	-
KKI	Philips Achieva	156	2500	30:14	72.70	8.1-12.8	97.4(19.4)	113.6(9.1)	12.8(4.0)
TRINITY	Philips Achieva	250	2000	24:23	100.00	12.0-25.9	108.9(15.3)	110.2(12.0)	10.7(2.8)
LEUVEN	Philips Intera	250	1667	33:28	90.20	12.1-32.0	109.4(13.1)	114.8(12.9)	-
SBL	Philips Intera	200	2200	14:14	100.00	22.0-64.0	109.2(13.6)	-	9.1(1.8)
NYU	Siemens Allegra	180	2000	104:72	80.10	6.5-39.1	107.8(16.6)	113.4(13.0)	11.1(4.1)
PITT	Siemens Allegra	200	1500	24:28	84.60	9.3-35.2	110.8(14.2)	110.0(9.0)	12.4(3.1)
OLIN	Siemens Allegra	210	1500	14:13	81.50	10.0-24.0	114.9(17.7)	118.1(14.1)	13.2(4.4)
UCLA	Siemens Tim Trio	120	3000	38:38	86.80	8.5-17.9	102.0(13.1)	107.0(10.1)	11.0(3.7)
USM	Siemens Tim Trio	240	2000	42:51	100.00	9.9-50.2	101.0(16.4)	115.0(13.9)	13.3(3.3)
YALE	Siemens Tim Trio	200	2000	28:25	71.70	7.0-17.8	94.8(21.9)	105.0(17.4)	-
CALTECH	Siemens Tim Trio	150	2000	14:7	71.40	17.0-56.2	106.2(13.6)	113.4(10.5)	14.3(4.2)
CMU	Siemens Verio	240	2000	13:10	78.30	19.0-40.0	114.8(12.2)	114.6(9.7)	13.4(3.5)
MAX_MUN	Siemens Verio	120	3000	30:19	85.70	7.0-52.0	109.4(15.7)	111.7(9.0)	9.0(4.4)
Total				496:393	84.40	6.5-64.0	106.1(17.0)	111.3(12.2)	11.9(3.8)

Results

Performance of the PINT Algorithm in ABIDE I

For most ABIDE I participants (55.6%), PINT converges on a solution after a median of 14 iterations (range 7-36). For remaining participants (44.4%), PINT starts oscillating between a handful of solutions within the same time frame (median 15; range 8-36 iterations). This oscillating behaviour is stopped when PINT reaches 50 iterations (the vertex solution iteration 50 is kept). These "oscillating" solutions (i.e. the vertices at iteration 50 vs the vertices at iteration 49) differed in the location of a median of 4 ROIs (range 1-19) by an average of 2.21mm each. This represents an average total of 1.27% of the total ROI displacement for that scan. Whether PINT converged to a single solution or began oscillating was not associated with the participants' diagnosis (chi-squared(1)=0.03, ns)

Whole Brain Network Correlation Maps

Supplemental Figures S1 and S2 show the seed correlation maps with the average timeseries from the network of interest calculated with template and personalized ROIs, respectively. The outlines of the Yeo et al. atlas (11) are plotted in white for each network. While the template ROIs used here are sampling only from 6mm circles in the center of the Yeo et al. atlas areas, the areas of higher correlation show strong visual correspondence with the Yeo seven network map. This correspondence remains for the personalized ROI derived correlation maps.

Supplemental Figure S1. Whole brain correlations with template vertex seeds.

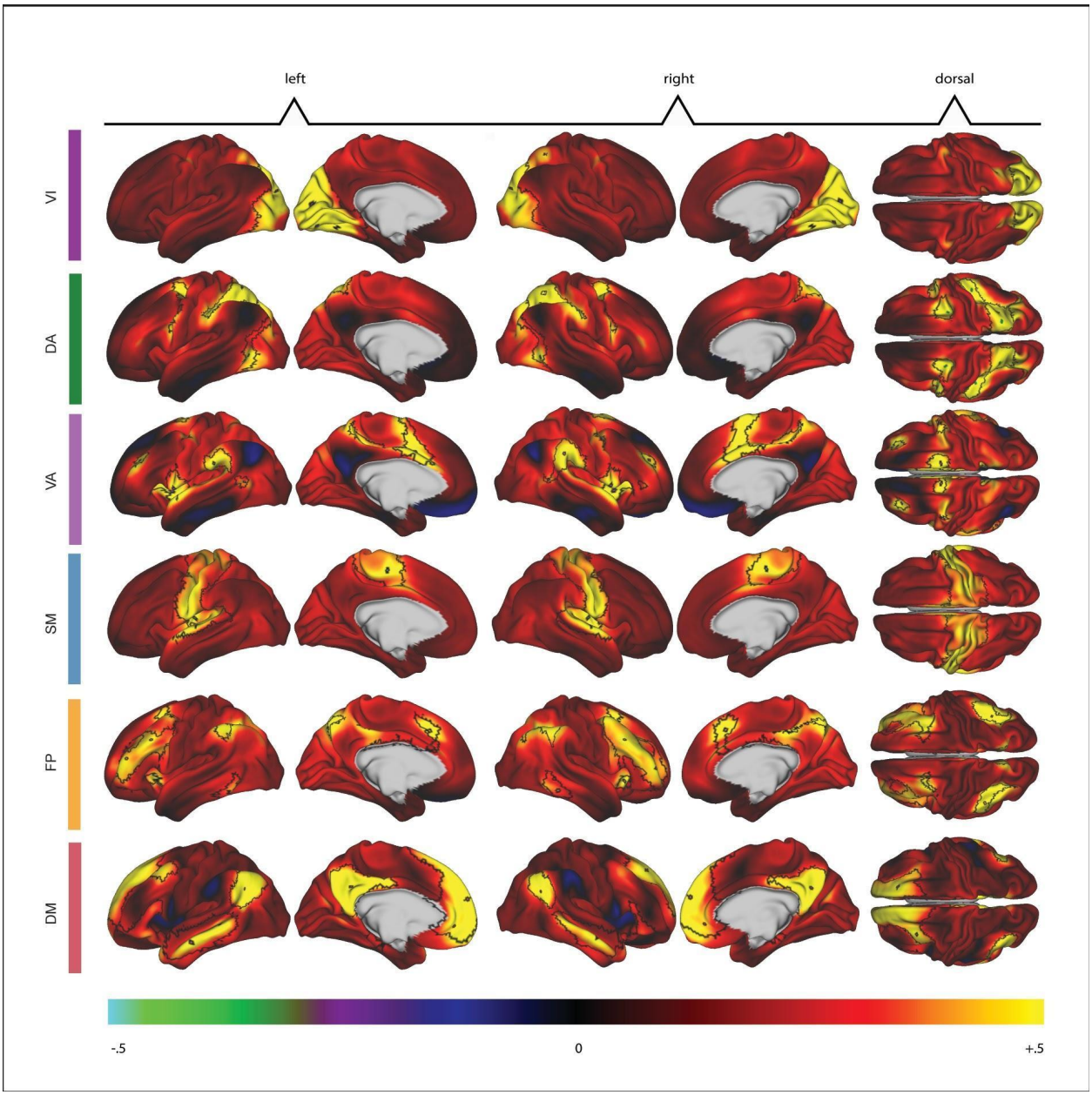

Supplemental Figure S2. Whole brain correlations with personalized vertex seeds.

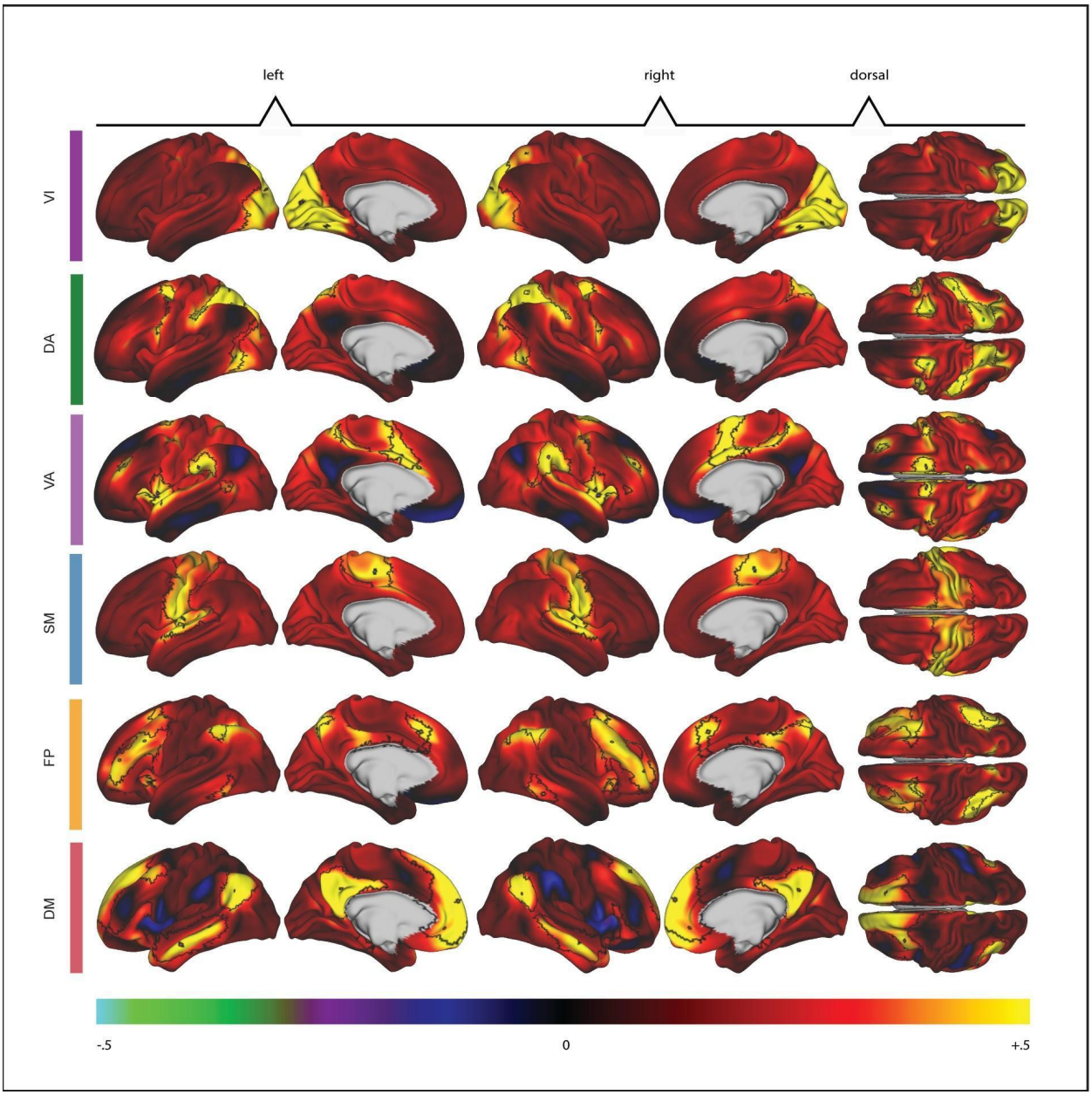

Supplemental Figure S3. Probabilistic maps of personalized ROI locations by network.

Color scale represents, for each vertex, the proportion of the ABIDE sample (n=889) where their 6mm radius personalized ROI encompassed that vertex. The Yeo et al. (2011) atlas outlines are also shown in white for reference. Note that the PINT algorithm was not given any information about the Yeo et al. (11) atlas borders. However, the final ROI locations tended to stay within the borders of the atlas.

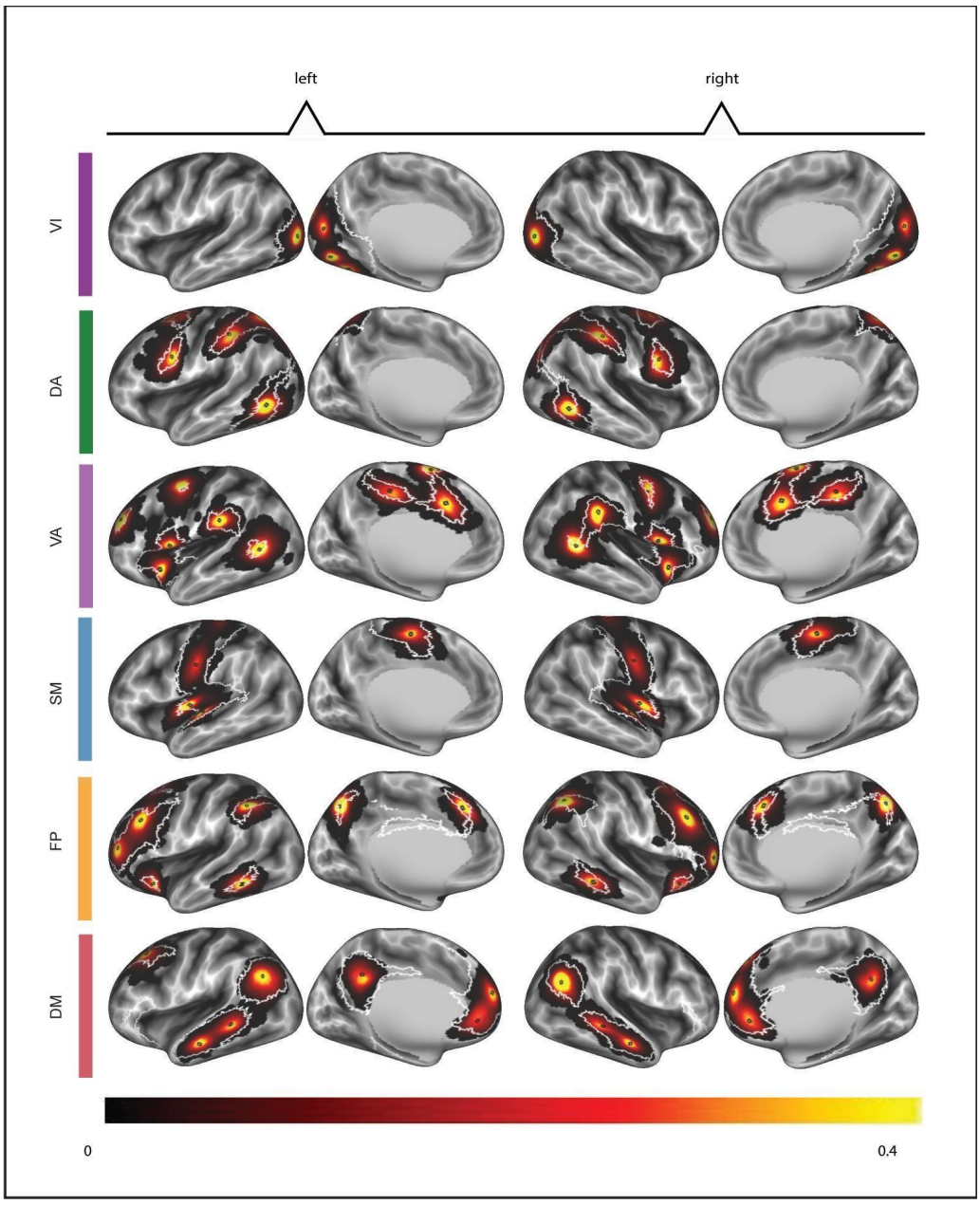

Supplemental Figure S4: No effect of in scanner head motion on PINT vertex displacement.

Scatter plots showing mean vertex displacement during PINT (mean of 80 ROIs) as a function of two measures for in-scanner motion (top) and mean framewise displacement (bottom) DVARS. Regressions are unadjusted (left) and adjusted (right) for the effects of scanning site.

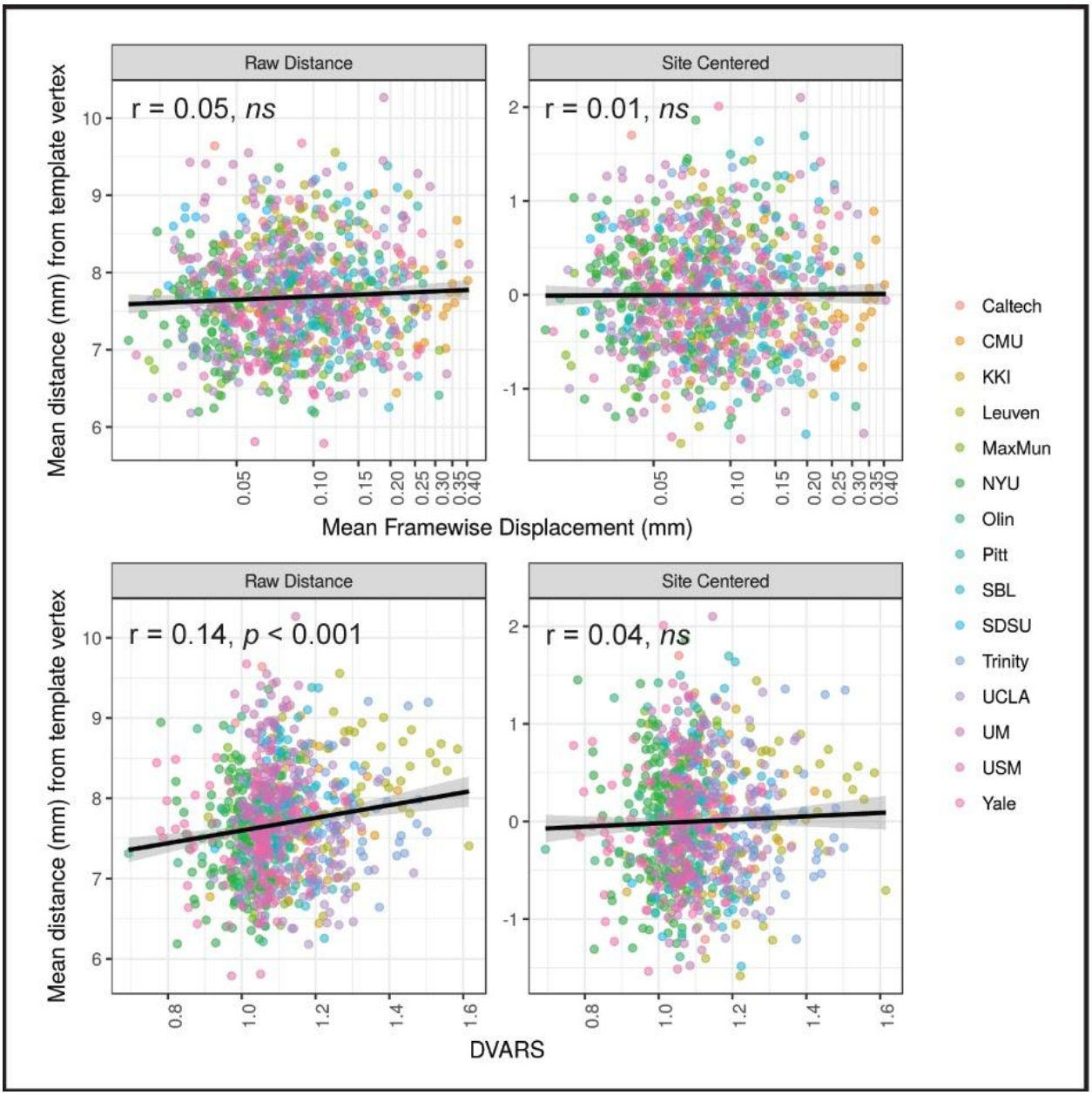

Supplemental Figure S5. Average correlation matrices (Z-transformed) from ABIDE I participants (n=889) calculated A) before PINT correlation ("template" ROIs) and B) after PINT correction ("personalized" ROIs).

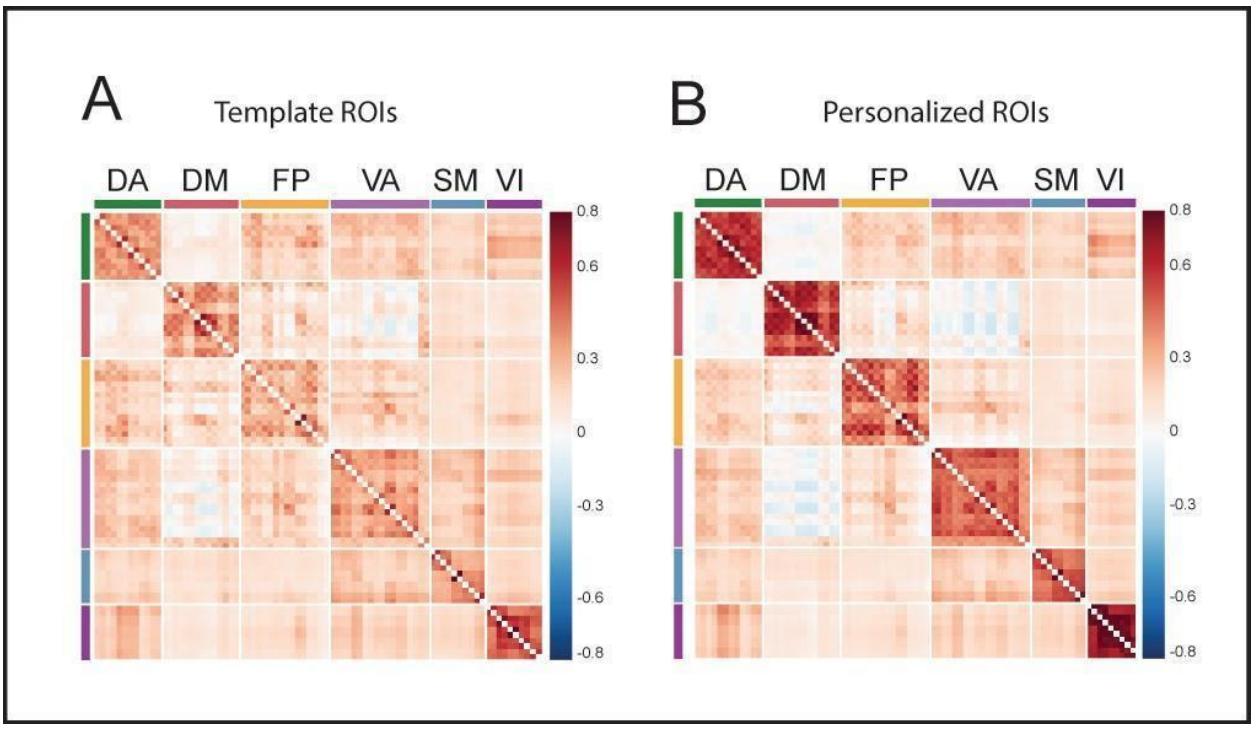

Supplemental Table S4. Mean (SD) network correlation (Z-transformed) from n=889 ABIDE I participants for template (Before PINT) and personalized (After PINT) ROIs.

	Within Network Correlation*			Between Network Correlation**		
Network	Template (Before PINT)	Personalized (After PINT)	Difference	Template (Before PINT)	Personalized (After PINT)	Difference
	M(SD)	M(SD)	M(SD)	M(SD)	M(SD)	M(SD)
All Edges						
VA	0.31(0.14)	0.45(0.18)	0.14(0.11)	0.16(0.10)	0.13(0.11)	-0.03(0.04)
DA	0.37(0.16)	0.60(0.20)	0.23(0.11)	0.17(0.10)	0.15(0.11)	-0.02(0.03)
DM	0.35(0.13)	0.59(0.18)	0.24(0.09)	0.09(0.10)	0.05(0.11)	-0.04(0.04)
FP	0.27(0.11)	0.45(0.15)	0.18(0.09)	0.15(0.10)	0.12(0.11)	-0.02(0.04)
SM	0.36(0.19)	0.50(0.24)	0.14(0.10)	0.16(0.11)	0.15(0.12)	-0.01(0.04)
VI	0.51(0.23)	0.73(0.26)	0.22(0.10)	0.16(0.10)	0.15(0.11)	-0.01(0.03)
Total	**0.34(0.12)**	**0.52(0.13)**	**0.19(0.05)**	**0.15(0.10)**	**0.12(0.10)**	**-0.02(0.02)**
Only Long Range connections (> 70mm apart on the Surface)						
VA	0.31(0.14)	0.45(0.18)	0.14(0.11)	0.15(0.10)	0.13(0.11)	-0.03(0.04)
DA	0.37(0.16)	0.60(0.20)	0.23(0.11)	0.17(0.10)	0.15(0.11)	-0.02(0.03)
DM	0.35(0.14)	0.59(0.18)	0.24(0.09)	0.09(0.10)	0.05(0.11)	-0.04(0.04)
FP	0.27(0.11)	0.44(0.15)	0.17(0.09)	0.14(0.10)	0.12(0.10)	-0.02(0.04)
SM	0.36(0.19)	0.49(0.24)	0.14(0.10)	0.16(0.11)	0.15(0.12)	-0.01(0.04)
VI	0.51(0.23)	0.72(0.26)	0.21(0.10)	0.15(0.10)	0.15(0.11)	-0.01(0.03)
Total	**0.33(0.12)**	**0.52(0.13)**	**0.18(0.05)**	**0.14(0.10)**	**0.12(0.10)**	**-0.02(0.02)**

* Within network correlation is defined as the mean correlation of ROIs with ROIs from the same network.

**Between network correlation is defined as the mean correlation of ROIs with those from a different network.

Supplemental Figure S6. Within ROI heterogeneity in resting state network correlation decreases with the application of PINT.

We measure spatial heterogeneity by calculating the standard deviation (across the vertices of an ROI) of that ROI's Z-transformed correlation with its own network.
***= p<0.001

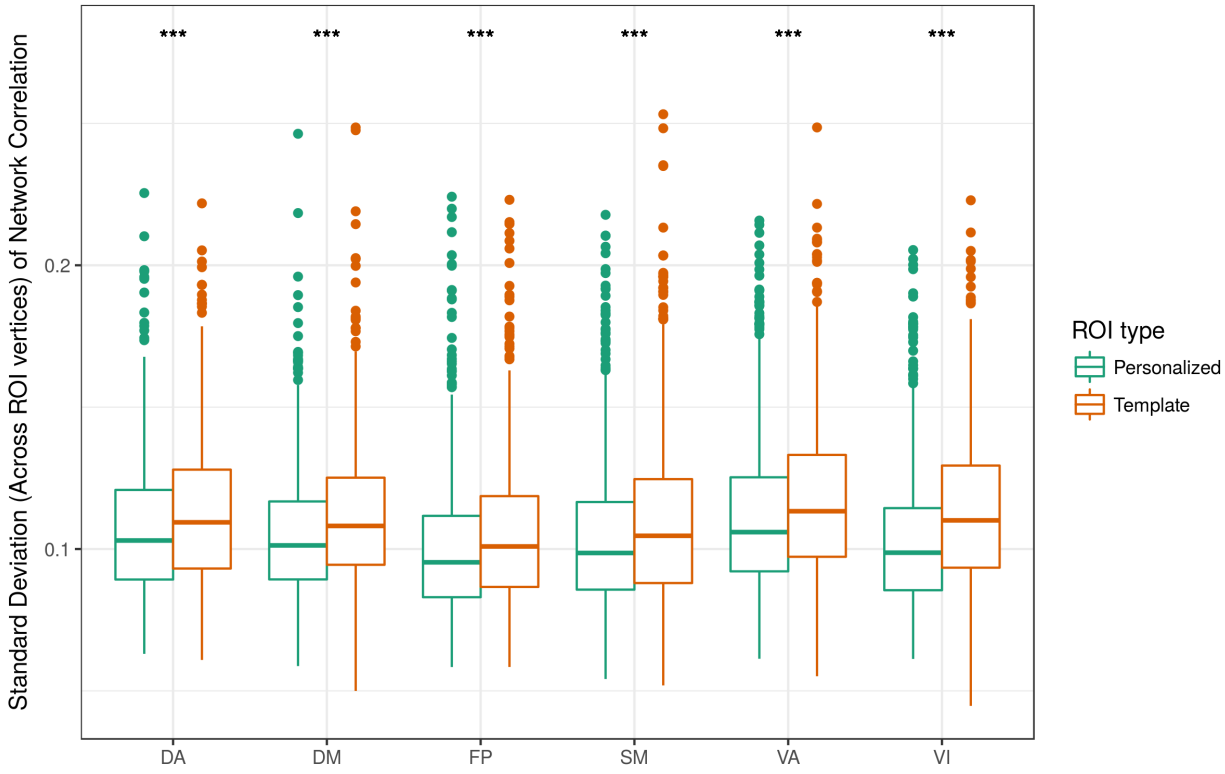

Supplemental Figure S7. Scatter plot of distance from each participant's personalized ROI location to the template vertex against age for both ASD and TD participants.

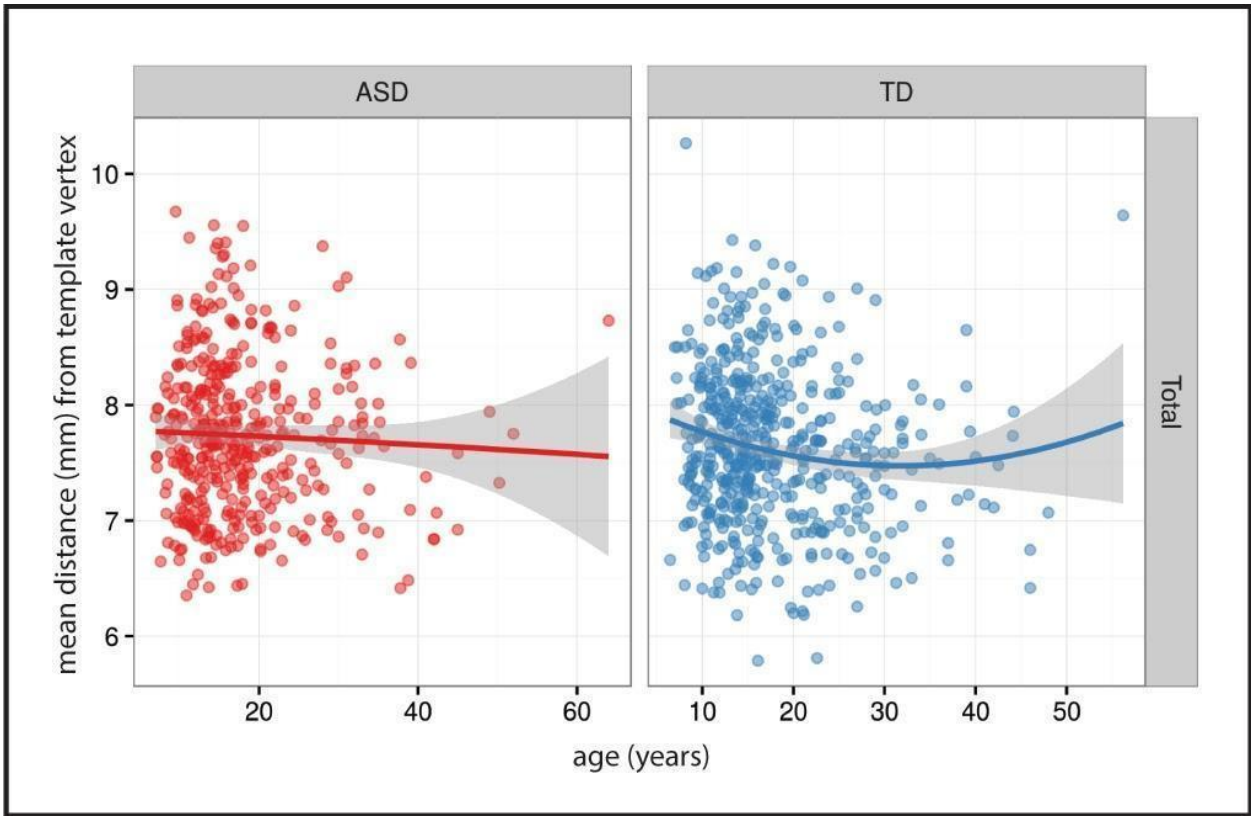

Supplemental Table S5. Association of ADOS total score with functional connectivity (n=264).

Edge	*t-statistic*	*p (uncorrected)*	*p (corrected)*	*r (raw)*	*r (adjusted)*
DMF2R.SAF5L	11.94	0.0006	--	-0.2075	-0.1699
DMF3L.SAF5L	19.25	0.0000	0.05	-0.2613	-0.2342
DMF3L.SAF5R	11.18	0.0010	--	-0.2032	-0.1674
DMF3L.SAP1L	12.47	0.0005	--	-0.2156	-0.1698
DMT1L.SAP1L	11.29	0.0009	--	-0.2039	-0.1513
DMT1R.EXF5L	11.52	0.0008	--	-0.2016	-0.1681
EXF4L.SAT1L	13.07	0.0004	--	-0.2144	-0.1769
EXT1L.VI04L	14.43	0.0002	--	-0.2211	-0.2181

Note. Adjusted r reflects adjustment for age, full IQ, site, gender, and fMRI quality control metrics. Corrected p values with FDR.

Supplemental Figure S8. Edges showing where a significant (FDR corrected) negative correlation between intrinsic connectivity and ADOS total scores was observed.

Plots were generated using nilearn (12).

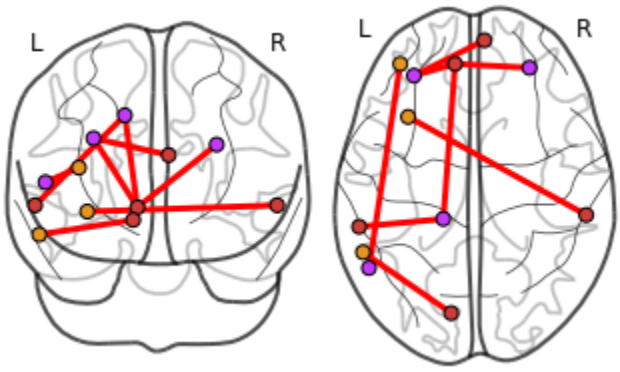

CoRR and ABIDE Longitudinal

Methods

Datasets

Test-retest performance and longitudinal stability of the PINT algorithm was tested using three datasets of TD individuals obtained from the Consortium for Reliability and Reproducibility (CORR; 13), of similar age and scan parameters as ABIDE: 1) NYU_2 (DOI: http://dx.doi.org/10.15387/fcp_indi.corr.nyu2, ages 8-55, n=187 retested same session, n=62 with 6 month follow-up), 2) University of Utah (Utah_1; DOI: http://dx.doi.org/10.15387/fcp_indi.corr.utah1, n=26, ages 8-38, scanned 2 years apart with a repeated scan in the second session), 3) University of Pittsburgh, School of Medicine (UPSM, DOI: http://dx.doi.org/10.15387/fcp_indi.corr.upsm1; n=100, ages 10-20, scanned 2 years apart). NYU_2 data was acquired on a Siemens Allegro scanner with EPI sequence parameters as follows: TR = 2000ms, TE = 15ms, 180 volumes, voxel size = 3 × 3 × 4mm^3, 33 interleaved slices, flip angle 90°, acquisition duration 6.00min. The Utah1 participants were scanned using a Siemens Tim Trio EPI sequence with parameters as follows: TR = 2000ms, TE = 28ms, 240 volumes, voxel size = 3.4 × 3.4 × 3 mm^3, 40 interleaved slices, flip angle 90°, acquisition duration 8:06min. The UPSM participants were scanned using a Siemens Tim Trio EPI sequence with parameters as follows: TR = 1500ms, TE = 29ms, 200 volumes, voxel size = 3.1 × 3.1 × 4 mm^3, 29 interleaved slices, flip angle 70°, acquisition duration 5.06min. Quality assurance pipeline outputs for these data were downloaded from the Consortia (13) (http://fcon_1000.projects.nitrc.org/indi/CoRR/html/qc.html). Scans were excluded if the field of view failed to capture the top of the head, or for excessive motion (greater than 25% of the timepoints having framewise displacement > 0.2mm).

From those scans available after quality assurance, two scans for each available participant were carried forward for each analysis (see Supplemental Table S5 for demographic criteria of the employed samples).

Supplemental Table S6. Demographic information from the CoRR participants employed in this analysis.

	UPSM	NYU_2		Utah_1	
	Longitudinal	**Same Session**	**Longitudinal**	**Same Session**	**Longitudinal**
N	44	135	53	23	16
Age at first scan (mean sd)	16.37 (2.14)	20.01 (9.99)	20.06 (10.51)	20.57 (8.39)	22.06 (7.95)
Sex (Count Male %)	22 (50.0%)	84 (62.2%)	30 (56.6%)	23 (100%)	16 (100%)
FIQ mean (sd)	Not reported	111.61 (12.24)	110.55 (11.55)	113.65 (14.63)	111.25 (14.76)
Days between scans	625.20 (150.98)	N/A	71.92 (65.63)	N/A	916.06 (81.50)

The longitudinal stability of the PINT algorithm was tested in the ABIDE Longitudinal sample, a release of two year follow-up scans from n=21 participants from UCLA and n= 17 participants from UPSM. The UCLA participants were scanned on a Siemens Tim Trio scanner with EPI sequence parameters as follows: TR = 3000ms, TE = 28ms, 120 volumes, voxel size = 3 × 3 × 4mm^3, 34 interleaved slices, flip angle 90°, acquisition duration 6.06min. The UPSM participants were scanned using a Siemens Allegro EPI sequence with parameters as follows: TR = 1500ms, TE = 25ms, 200 volumes, voxel size = 3.1 × 3.1 × 4 mm^3, 29 interleaved slices, flip angle 70°, acquisition duration 5.06min.

Preprocessing Workflow

MR preprocessing workflow is the same as employed for ABIDE I and is described in the Technical Methods: Preprocessing Pipeline section, with the exception that the CoRR datasets' surfaces were define using FreeSurfer v.6.0.0 (instead of v5.3.0). Due to the poor quality of anatomical scans from some UCLA participants, the FreeSurfer outputs from each subject's higher quality timepoint (12 baseline, 9 follow-up) were used for all subsequent analyses of the same participant. For all other data, all scans were of sufficient quality such that the resting state data was mapped to the anatomical data collected within the same session.

Test-Retest Analysis of Resting State Connectivity

We extracted average timeseries from the 6mm circular ROIs at both template locations and personalized locations. From these timeseries, within scan, Z-transformed correlation matrixes were calculated. We vectorized these timeseries and cross-correlated them between scans to build a "cross" scan correlation matrix. This matrix was decomposed into 'within-subject' and 'mean-cross-subject' similarity scores for each ROI. Within-subject is the correlation between the same participant's correlation matrix from baseline to follow-up, and cross-subject is the mean of one participant's baseline correlation matrix values to all other participants' follow-up correlation matrices from the same site. Additionally, I2C2 was calculated as an additional measure of test-retest reliability for both template and personalized ROI correlation matrices (14).

Supplemental Figure S9. Between-subject and within-subject distance for personalized ROI locations by network.

*p<0.05, **p<0.01, ***p<0.001

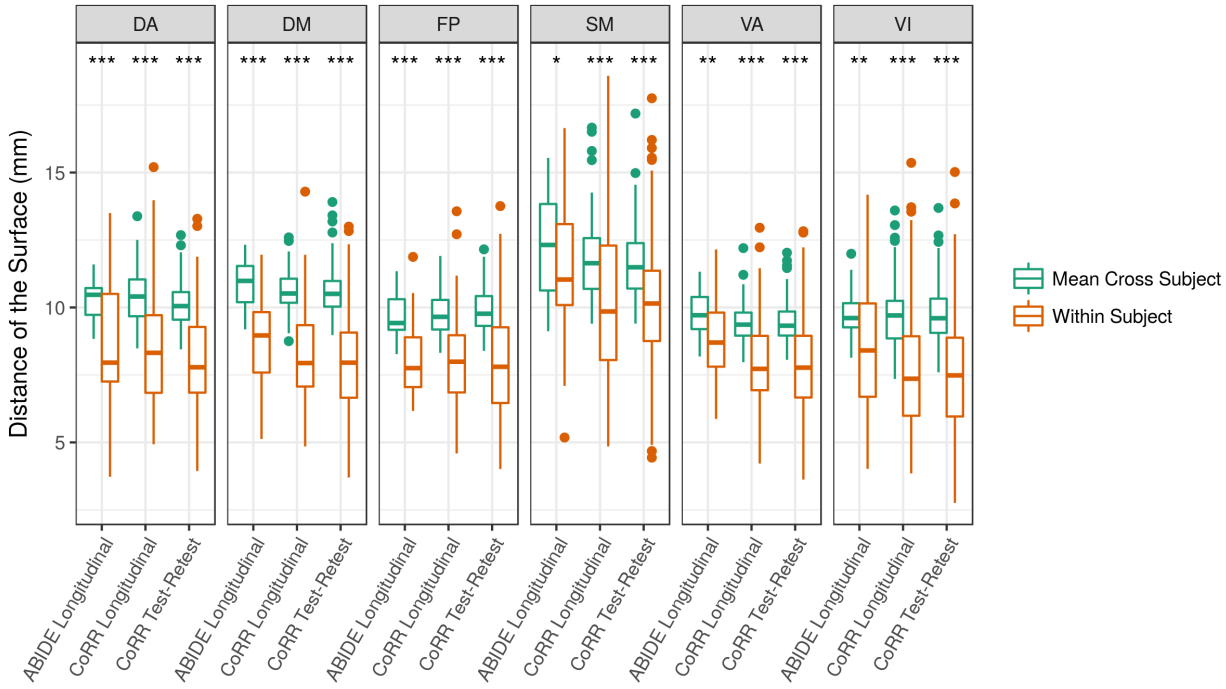

Supplemental Table S7. Paired t-test results for within-subject and between-subject distances of PINT personalized ROI locations across site and diagnosis.

			Mean (SD)		
Site	Group	n	Cross Participant	Within Participant	Paired t-test
UCLA	ASD	9	10.4(0.3)	9.6(0.7)	t(8)=4.81, p=0.001
UCLA	TD	5	10.3(0.2)	8.7(0.7)	t(4)=4.60, p=0.01
UPSM	ASD	9	10.4(0.5)	8.8(1.1)	t(8)=5.33, p=0.0007
UPSM	TD	8	10.2(0.6)	8.6(0.9)	t(7)=6.20, p=0.0004

Supplemental Table S8. Comparison of within subject and cross subject correlation matrices, before and after PINT.

The final correlation matrices produced from the 80 personalized ROI timeseries were more similar within-subject compared to cross-subject in all datasets tested. However, it should be noted that the within-subject to cross-subject difference was greater for correlation matrices calculated on the original template ROI locations compared to the personalized ROI locations. As a result, test-retest reliability (measured as intra-class correlation or I2C2 (14)) was higher for template ROIs than personalized ROIs. This was expected, as the PINT algorithm increased the within-subject correlation, but also the cross-subject correlation (i.e., it makes participants' correlation matrices more similar).

	n	I2C2 (95% CI)	Cross Scan Correlation (Z) Mean (SD)			Paired t-test (Within vs Cross)
			Within Subject	Cross Subject	Difference	
Personalized ROIs						
CoRR datasets						
Utah Test-Retest	23	0.30 (0.23-0.37)	0.67(0.15)	0.50(0.06)	0.17(0.13)	$t(22)=6.26$, $p<10^{-5}$
Utah Long.	16	0.23 (0.18-0.26)	0.63(0.15)	0.55(0.09)	0.09(0.09)	$t(15)=3.75$, $p=0.002$
NYU Test-Retest	135	0.25 (0.22-0.28)	0.63(0.16)	0.48(0.07)	0.15(0.13)	$t(134)=13.40$, $p<10^{-25}$
NYU Long.	53	0.23 (0.18-0.26)	0.62(0.15)	0.48(0.08)	0.14(0.11)	$t(52)=9.43$, $p<10^{-12}$
UPSM Long.	44	0.15 (0.08-0.21)	0.55(0.11)	0.46(0.05)	0.09(0.10)	$t(43)=6.00$, $p<10^{-6}$
ABIDE Longitudinal Sites						
UCLA Long.	14	0.17 (0.13-0.21)	0.53(0.09)	0.44(0.06)	0.09(0.10)	$t(13)=3.57$, $p=0.003$
UPSM Long.	17	0.21 (0.12-0.30)	0.58(0.09)	0.49(0.05)	0.09(0.06)	$t(16)=5.50$, $p<10^{-4}$
Template ROIs						
CoRR datasets						
Utah Test-Retest	23	0.45 (0.39-0.50)	0.65(0.15)	0.31(0.05)	0.34(0.13)	$t(22)=12.94$, $p<10^{-11}$
Utah Long.	16	0.32 (0.29-0.36)	0.56(0.16)	0.34(0.07)	0.23(0.11)	$t(15)=8.39$, $p<10^{-6}$
NYU Test-Retest	135	0.35 (0.31-0.39)	0.56(0.16)	0.28(0.05)	0.28(0.13)	$t(134)=25.58$, $p<10^{-52}$
NYU Long.	53	0.32 (0.29-0.36)	0.54(0.14)	0.28(0.06)	0.26(0.11)	$t(52)=17.66$, $p<10^{-22}$
UPSM Long.	44	0.23 (0.17-0.30)	0.47(0.11)	0.27(0.04)	0.20(0.09)	$t(43)=13.82$, $p<10^{-16}$
ABIDE Longitudinal Sites						
UCLA Long	14	0.25 (0.19-0.31)	0.41(0.10)	0.23(0.05)	0.18(0.08)	$t(13)=8.24$, $p<10^{-5}$
UPSM Long	17	0.31 (0.24-0.39)	0.50(0.07)	0.30(0.05)	0.20(0.06)	$t(16)=13.05$, $p<10^{-9}$

Evaluation of PINT Parameters on Test-Retest Performance

Methods

We evaluated specific PINT parameters in terms of test-retest reliability in two CoRR datasets (NYU n = 135 and Utah n = 23). Three parameters, used by the PINT algorithm were evaluated.

- **Search Radius:** This radius limits the distance that any vertex can move within one iteration of PINT (values tested: 4, 6, 8, 10 mm).
- **Padding Radius:** This limits the distance between adjacent ROIs (values tested: 10, 12, 14 mm).
- **Sampling Radius:** The size of the radius for mean timeseries extraction (values tested: 4, 5, 6, 10 mm).

Two measures of test-retest reliability were examined. In both cases, we use "distinctiveness" as our measure. This measure, which closely relates to the “fingerprint” test (15), is computed by comparing the similarity (or distance) of one participant with their own retest-scan to that of one participant’s scan with all the retest scans within the dataset. This is expressed as a Z-score (i.e. where on the distribution of all (within and between) subject similarities does the within subject similarity fall). Higher values are better, as they would increase the likeliness of passing the "fingerprint" test. The two measures of similarity were:

1. **PINT Location "distinctiveness"** calculated from test-retest distances between the locations of the PINT ROIs. Measured using the mean geodesic distance (on the HCP S1200 Average mid thickness surface) between the PINT output vertices of two scans. Distance is averaged across the 80 ROIs. In its “raw” form, lower negative values represent more test-retest “distinctiveness” values. For easier interpretation and comparison with other measure, values were multiplied by -1 (i.e. larger positive represent more test-rested “distinctiveness”).

2. **Personalized Correlation Matrix "distinctiveness**" of the similarity of the correlation matrices from individual scans. Pearson correlation of the vectorized Z-transformed upper triangle of the correlation matrix computed from the personalized vertices (similar to the measure used in (15)).

Results

PINT location distinctiveness and personalized correlation distinctiveness were combined into a test-retest score for every participant (using the sum of their squares). These three measures are plotted (mean ± standard error) as a function of sampling radius, search radius, and padding radius. The top ranking combination of parameters was: search radius = 6mm, padding radius = 12mm, sampling radius = 10mm. To understand these trends further, PINT location "distinctiveness" and personalized correlation matrix "distinctiveness" were used as dependent variables in a linear mixed model analysis with search radius, padding radius, and sampling radius as linear fixed effects and with subject and scanner (NYU vs Utah) as random intercepts. In general, we observed that the padding radius had negligible effects on either measure (PINT locations: $t = -1.58$, $p = 0.11$, personalized correlation matrix: $t = -1.18$, $p = 0.24$). Search radius had opposing effects on either measure: with increasing search radius we observed lower personalized correlation matrix distinctiveness ($t = -18.88$, $p < 10^{-16}$) but higher PINT location distinctiveness ($t = 11.68$, $p < 10^{-16}$). A search radius of 6mm or 8mm appeared to be the best compromise of the two factors. The higher sampling radius was associated with increased correlation matrix distinctiveness ($t = 32.5$, $p < 10^{-16}$), and a lessened beneficial effect on location distinctiveness ($t = 2.51$, $p = 0.01$).

Supplemental Figure S10: Evaluating the effects of PINT input parameters on test-retest reliability of PINT results (n=158 test-retest participants).

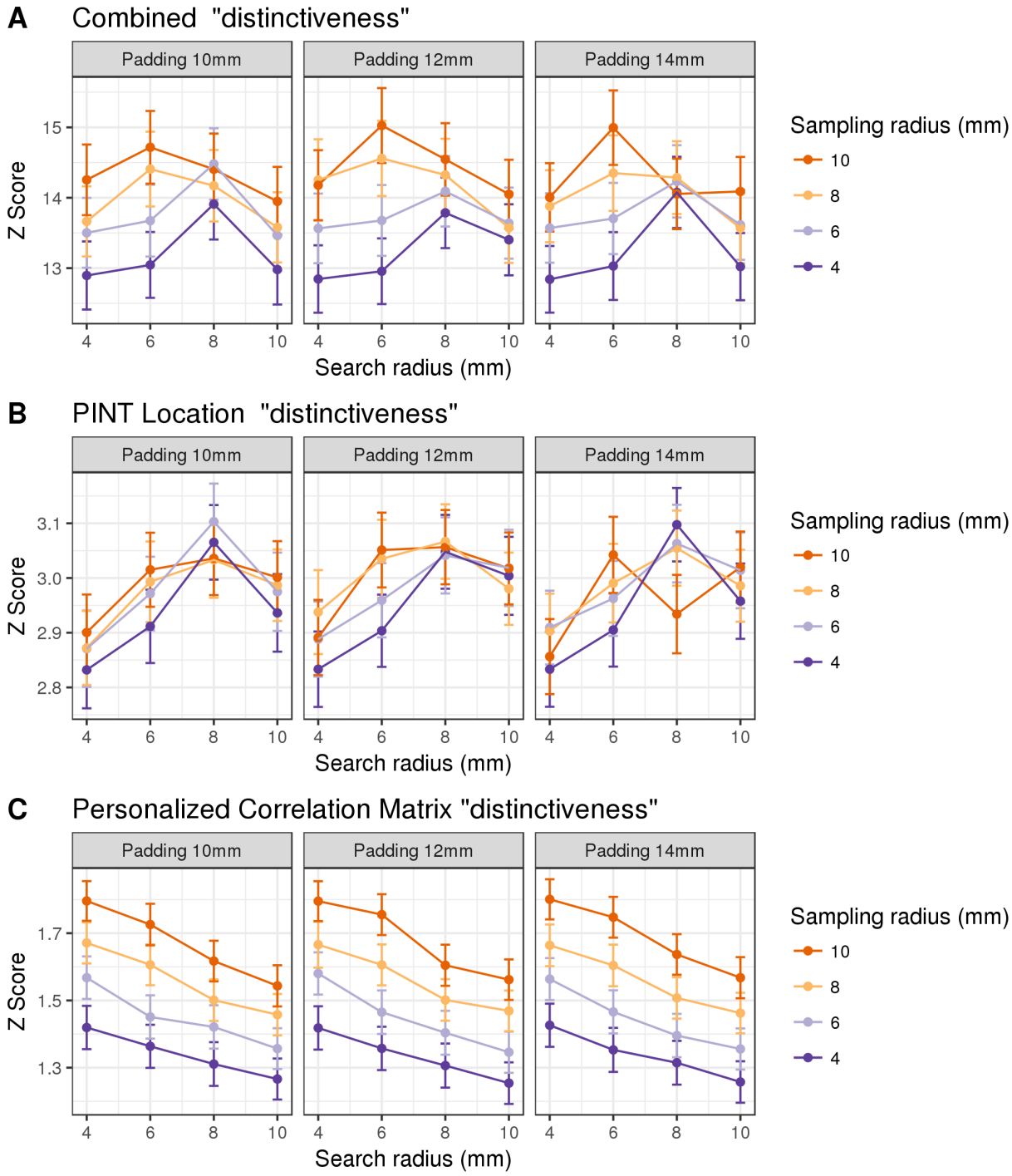

Taken together, these test-retest analyses lend more confidence to our use of a search radius of 6mm and a padding radius of 12mm in the analyses reported throughout this manuscript. They also suggest that it may have been beneficial to increase the sampling radius from 6mm to 8mm or 10mm. We therefore conducted PINT analyses in the ABIDE I sample using 8mm and 10mm search radii. The main results for our manuscript remained unchanged in both cases. Specifically, we found greater variability in the spatial locations of resting state networks within individuals with ASD as compared to TD. Comparison of intrinsic connectivity between groups revealed that the application of PINT decreased the number of hypo-connected regions in ASD.

Table S9. Effects of ASD Diagnosis on vertex displacement and functional correlations after varying the PINT sampling radius settings.

	Effect of Diagnosis on Vertex Displacement	Effect of ASD Diagnosis on functional correlation (Number of significant edges FDR corrected)		
PINT Sampling Radius		Template Hypo/Hyper	Personalized Hypo/Hyper	Difference Hypo/Hyper
6mm	t=-3.23, p=0.001	214/0	80/4	-134/+4
8mm	t = -2.67, p=0.008	295/0	125/7	-170/+7
10mm	t=-2.53, p = 0.01	373/0	296/9	-77/+9

Supplemental Figure S11. Maximizing full correlation within the PINT algorithm increases the correlation (adjusted for scanning site and age) between functional connectivity and head-motion (mean framewise displacement), but maximizing partial correlation does not increase correlation between functional connectivity and head motion.

The distribution of median (n=889 ABIDEI participants) edgewise correlations between functional correlation values and head motion (mean framewise displacement) are plotted for correlation matrices from Template (orange) and Personalized (green) calculated after PINT was run maximizing full correlation (top) and partial correlation (bottom). After maximizing full correlation the median correlation across edges, between functional correlation across subjects and head motion (measured as mean framewise displacement) increased substantially (Template median correlation: r = 0.10, Personalized median correlation: r = 0.17, $t(6253) = 60.7$, $p < 10^{-1449}$). These results suggest that when PINT maximizes full correlation, it could be moving the ROIs to locations toward extreme values caused by head motion. This was not the case when maximizing partial correlation (accounting for the 5 other network timeseries). When PINT maximizes partial correlation, the median correlation between functional correlation and motion decreased slightly (Template median correlation: r = 0.10, Personalized median correlation: r = 0.09, $t(6269) = -11.22$, $p < 10^{-52}$). Note that all results reported in this manuscript use the "maximizing partial correlation" variant of PINT.

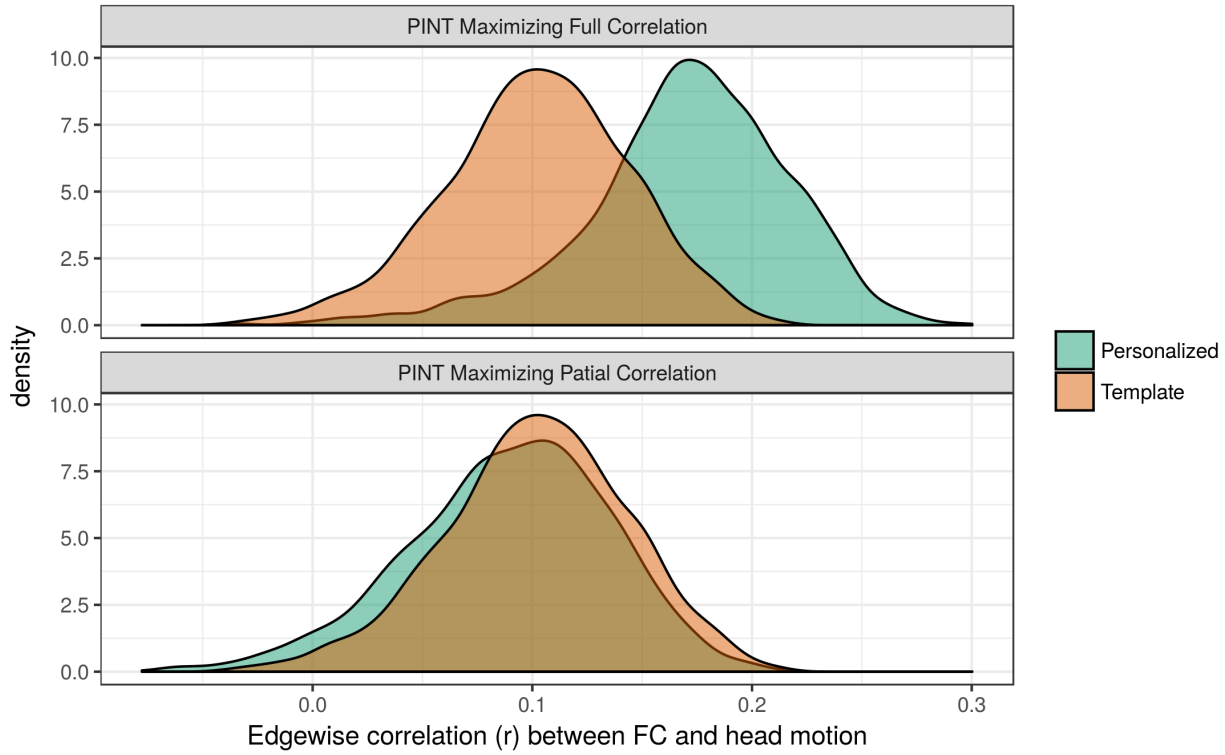

Supplemental References

1. Fischl B (2012): FreeSurfer. *Neuroimage*. 62: 774–781.

2. Glasser MF, Sotiropoulos SN, Wilson JA, Coalson TS, Fischl B, Andersson JL, *et al.* (2013): The minimal preprocessing pipelines for the Human Connectome Project. *Neuroimage*. 80: 105–124.

3. Jenkinson M, Beckmann CF, Behrens TEJ, Woolrich MW, Smith SM (2012): FSL. *Neuroimage*. 62: 782–790.

4. Cox RW (1996): AFNI: Software for Analysis and Visualization of Functional Magnetic Resonance Neuroimages. *Comput Biomed Res*. 29: 162–173.

5. Salimi-Khorshidi G, Douaud G, Beckmann CF, Glasser MF, Griffanti L, Smith SM (2014): Automatic denoising of functional MRI data: Combining independent component analysis and hierarchical fusion of classifiers. *Neuroimage*. 90: 449–468.

6. Power JD, Barnes KA, Snyder AZ, Schlaggar BL, Petersen SE (2012): Spurious but systematic correlations in functional connectivity MRI networks arise from subject motion. *Neuroimage*. 59: 2142–2154.

7. Fox MD, Liu H, Pascual-Leone A (2013): Identification of reproducible individualized targets for treatment of depression with TMS based on intrinsic connectivity. *Neuroimage*. 0: 151–160.

8. Chen T, Ryali S, Qin S, Menon V (2013): Estimation of resting-state functional connectivity using random subspace based partial correlation: a novel method for reducing global artifacts. *Neuroimage*. 0: 87–100.

9. Power JD, Schlaggar BL, Petersen SE (2015): Recent progress and outstanding issues in motion correction in resting state fMRI. *Neuroimage*. 0: 536–551.

10. Di Martino A, Yan C-G, Li Q, Denio E, Castellanos FX, Alaerts K, *et al.* (2014-6): The Autism Brain Imaging Data Exchange: Towards Large-Scale Evaluation of the Intrinsic Brain Architecture in Autism. *Mol Psychiatry*. 19: 659–667.

11. Yeo BTT, Krienen FM, Sepulcre J, Sabuncu MR, Lashkari D, Hollinshead M, *et al.* (2011): The organization of the human cerebral cortex estimated by intrinsic functional connectivity. *J Neurophysiol*. 106: 1125–1165.

12. Abraham A, Pedregosa F, Eickenberg M, Gervais P, Mueller A, Kossaifi J, *et al.* (2014): Machine learning for neuroimaging with scikit-learn. *Front Neuroinform*. 8. doi: 10.3389/fninf.2014.00014.

13. Zuo X-N, Anderson JS, Bellec P, Birn RM, Biswal BB, Blautzik J, *et al.* (2014): An open science resource for establishing reliability and reproducibility in functional connectomics. *Sci Data*. 1: 140049.

14. Caceres A, Hall DL, Zelaya FO, Williams SCR, Mehta MA (2009): Measuring fMRI reliability with the intra-class correlation coefficient. *Neuroimage*. 45: 758–768.

15. Finn ES, Shen X, Scheinost D, Rosenberg MD, Huang J, Chun MM, *et al.* (2015): Functional

connectome fingerprinting: identifying individuals using patterns of brain connectivity. *Nat Neurosci*. 18: 1664–1671.